

Ferromagnetism in armchair graphene nanoribbon heterostructures

P. A. Almeida , L. S. Sousa, Tome M. Schmidt, and G. B. Martins 

Instituto de Física, Universidade Federal de Uberlândia, Uberlândia, Minas Gerais 38400-902, Brazil



(Received 3 November 2021; revised 23 January 2022; accepted 9 February 2022; published 17 February 2022)

We study the properties of flat bands that appear in a heterostructure composed of strands of different widths of graphene armchair nanoribbons. One of the flat bands is reminiscent of the one that appears in pristine armchair nanoribbons and has its origin in a quantum mechanical destructive interference effect, dubbed “Wannier orbital states” by Lin *et al.* in *Phys. Rev. B* **79**, 035405 (2009). The additional flat bands found in these heterostructures, some reasonably closer to the Fermi level, seem to be generated by a similar interference process. After doing a thorough tight-binding analysis of the band structures of the different kinds of heterostructures, focusing on the properties of the flat bands, we use density functional theory to study the possibility of magnetic ground states when placing, through doping, the Fermi energy close to the different flat bands. Our DFT results confirmed the expectation that these heterostructures, after being appropriately hole doped, develop a ferromagnetic ground state that seems to require, as in the case of pristine armchair nanoribbons, the presence of a dispersive band crossing the flat band. In addition, we found a remarkable agreement between the tight-binding and DFT results for the charge density distribution of the so-called Wannier orbital states.

DOI: [10.1103/PhysRevB.105.054416](https://doi.org/10.1103/PhysRevB.105.054416)

I. INTRODUCTION

Strong correlations in magic-angle twisted bilayer graphene (TBG), discovered in 2018 [1] (see Ref. [2] for a review), were associated with the presence of strongly correlated states in flat minibands of the hexagonal Moiré superlattice, as previously predicted by band structure calculations [3–5]. Recently, ARPES measurements [6] have provided direct evidence for the existence of flat bands in magic-angle TBG. These developments have greatly increased the interest in the study of low-dimensional systems presenting bands with zero (or quasizero) dispersion.

Indeed, in the last one year alone, there has been new flat-band research in many different areas, like their experimental observation in atomically precise one-dimensional (1D) chains [7], as well as the study of flat bands in strongly correlated systems [8–16], search for flat bands in kagome-type lattices [17,18], study of symmetry aspects of flat-band systems [19–21], holographic construction of flat bands [22], flat bands in pyrochlore lattices [23,24], analysis of randomness in flat-band Hamiltonians [25], topological aspects of flat-band systems [26–31], construction of flat-band tight-binding models starting from compact localized states [32], and study of flat bands in graphene and graphenelike lattices [33–37].

For a brief review of the research in flat bands, describing initial theoretical proposals in the late 1980s [38,39], their association with topological phases [40,41], and their possible realization in superconducting wire networks, cold atoms in optical lattices, and photonic systems, see Ref. [42]. For a description of strongly correlated ground states associated with dispersionless bands, see Ref. [43].

Following the development of a bottom-up procedure for atomically precise synthesis of semiconducting graphene

nanoribbons (GNRs) with different width, edge, and end termination [44], a seminal paper by Louie’s group in 2017 [45] showed that these synthesized armchair GNRs (AGNRs) strands belonged to different topological phases, protected by spatial symmetries and with a Z_2 topological invariant whose value was dictated by their width and terminating unit cell. Thus, the bulk-boundary correspondence principle [46–51] imposes that at the interface between two finite AGNRs, with different Z_2 values, a topologically protected localized state should exist, with its energy located inside the AGNR gap. This expectation was confirmed by density functional theory (DFT) calculations [45]. The following year, two experimental groups, one in Europe [52] and the other in the USA [53], published side-by-side Nature papers presenting DFT and tight-binding simulations of scanning tunneling spectroscopy (STS) measurements in superlattices of short AGNR strands, alternating between finite and vanishing Z_2 values that indicated the presence, inside the (overall) AGNR gap, of a dimerized chain band structure. A Su-Schrieffer-Heeger (SSH) effective model (initially proposed to describe polyacetylene [54], and recently revived as a prototypical model for a one-dimensional topological insulator [55]), was shown to qualitatively describe the experimental results. Thus, in what was described as a *hierarchically engineered one-dimensional topological system* [52], the AGNR heterostructure, with topologically nontrivial properties (i.e., a topologically protected end state), is itself composed of alternating topologically trivial and nontrivial building blocks. Besides the ability of considerably decreasing the AGNR’s spectral gap (with the recent observation of metallicity in an AGNR heterostructure [56]—notice that all AGNRs are actually semiconducting [57]), the properties of these heterostructures, as implied by the results presented in

Refs. [52,53], have generated much attention, as they represent one of the first stable materials (besides polyacetylene) that simulates the SSH model, which up to now had been simulated mainly in cold-atom [58], engineered atomic lattices [59,60], photonic [61], acoustic [62], and mechanical [63,64] experimental configurations. Very recent work, extending the results in Refs. [52,53], may be found in Refs. [65,66].

A much less studied aspect of these AGNR heterostructures is the presence of dispersionless bands in their band structure. In this work, using the tight-binding method and DFT, we systematically analyze how the presence or not of flat bands, their proximity to the Fermi energy, their interplay with nearby dispersive bands, as well as if they give origin or not to a ferromagnetic ground state, depends on the parameters that define the AGNR heterostructure. Our results show that, indeed, the majority of the heterostructures studied through tight-binding present several flat bands that can be associated with “Wannier orbital” states, as formerly seen in pristine AGNRs [67]. By appropriately hole doping these heterostructures, i.e., bringing the Fermi energy close to a flat band, a ferromagnetic ground state is observed through DFT simulations. The ferromagnetic exchange coupling at the flat band appears to be mediated by a dispersive band that crosses it [67].

We want to emphasize that we did not investigate the topological properties of the heterostructures studied here. However, in the discussion of the results, possible connections between ferromagnetism and the SSH effective model were pointed out to motivate further research on that particular aspect.

The organization of the paper is as follows: In Sec. II we introduce the AGNR heterostructure parameters N , n , and m , together with the tight-binding Hamiltonian that models it, while in Sec. III, to illustrate the appearance of flat bands in these heterostructures, we present the tight-binding results for heterostructures with the second smallest unit cell, i.e., $N = 3$, $n = 1$, and $m = 3$, showing the presence of four valence flat bands (with respective particle-hole symmetric conduction band partners). Then, in Sec. IV, we show that flat bands survive for “backbones” $N = 5$ and $N = 7$, and also present the profile of the Wannier orbital states associated with each one of the four lowest energy flat bands. For $N = 9$, the flat bands present for smaller values of N acquire dispersion. In Sec. V, we keep $N = 3$ and vary the other two parameters, n and m , and analyze their influence over the flat bands and the corresponding Wannier orbital states (which, from now on, will be called Wannier-like states). This will set the stage for an *ab initio* DFT analysis of the ferromagnetic ground state present for varying hole doping in Sec. VI. Finally, in Sec. VIII we present a summary of the results obtained and our concluding remarks. For completeness sake, in Appendix A we present the Hamiltonian in real and reciprocal space for an N -AGNR(1,3) heterostructure (see next section, for notation). In addition, in Appendixes B and C we discuss the effects of adding a next-nearest-neighbor (NNN) hopping to the main-text tight-binding calculations and briefly present tight-binding and DFT band structures for an alternative (less symmetric) type of heterostructure that has also been synthesized in the laboratory [52,53].

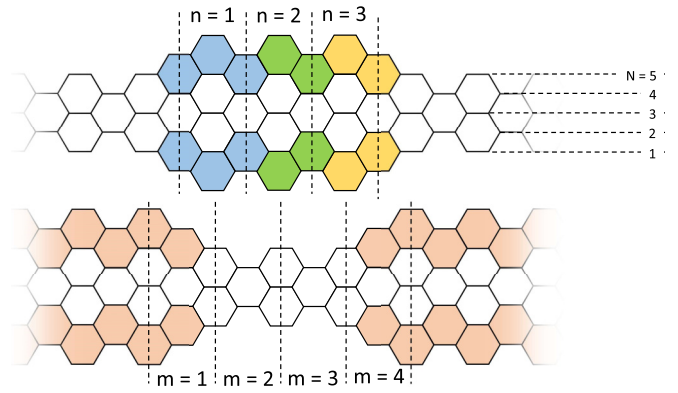


FIG. 1. Schematic representation of the meaning of the parameters N , n , and m in an N -AGNR(n, m) heterostructure. See text for details.

II. MODEL FOR THE HETEROSTRUCTURES

A. The geometry of the N -AGNR(n, m) heterostructures

In Ref. [53], two types of AGNR heterostructures were introduced, the so-called “inline” and “staggered” heterostructures. In this paper we will analyze the properties just of inline heterostructures (which we will name N -AGNR(n, m) heterostructures), since they present more flat bands than the staggered heterostructures.

In Fig. 1 we schematically show how the unit cell of an N -AGNR(n, m) heterostructure is built. In the top panel, the parameter n indicates how many adjacent unit cells (delimited by vertical dashed lines) of the so-called backbone (a pristine N -AGNR, depicted in white), containing $N = 5$ dimers in each unit cell, as indicated in the right, will be extended into unit cells containing $N + 4$ dimers. As indicated in Fig. 1, this is done, for the first of the n unit cells, by adding six extra carbons to the top and bottom of the unit cell. This adds three extra benzene rings, colored in cyan, to the top and bottom of the unit cell. To extend the next unit cell (adjacent to the right), just four extra carbon atoms are needed to add two more benzene rings, colored in green. This second step is repeated until all n adjacent unit cells are extended. The top panel in Fig. 1 shows the result for $n = 3$. Finally, in the bottom panel, m indicates how many unit cells away from the last extended unit cell we will repeat the process of extending n unit cells. There is an important detail here: we count m from the center of the last extended unit cell to the center of the first extended unit cell of the next n group to the right (notice the positioning of the vertical dashed lines in the bottom panel, see Fig. S2 in Ref. [53]). Therefore, the unit cell of the N -AGNR(n, m) heterostructure thus obtained will contain $n + m - 1$ unit cells of the original backbone. It is clear that $m \geq 2$, since $m = 1$ produces a uniform AGNR with a width equal to $N + 4$.

B. Tight-binding Hamiltonian

The band structure of these N -AGNR(n, m) heterostructures will be simulated using a tight-binding Hamiltonian

$$H_{\text{tb}} = -t \sum_{(i,j)\sigma} c_{i\sigma}^\dagger c_{j\sigma}, \quad (1)$$

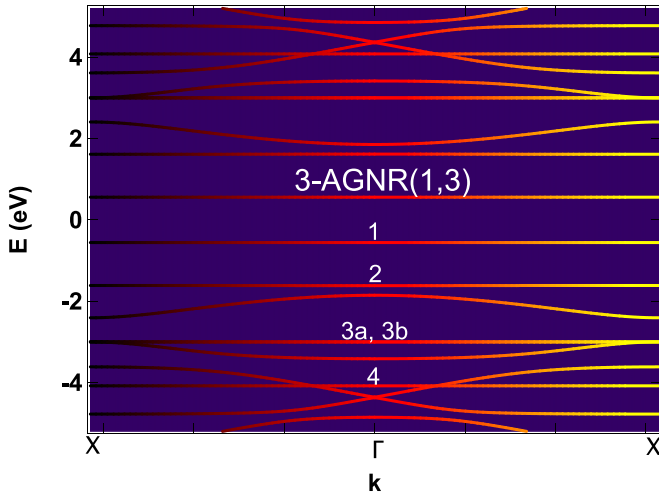


FIG. 2. Tight-binding band structure of a 3-AGNR(1,3) heterostructure. The flat bands are indicated by labels 1, 2, 3a, 3b, and 4, starting from the Fermi energy at half-filling ($E = 0$). Note that band 3 is double degenerate.

where $c_{i\sigma}^\dagger$ ($c_{i\sigma}$) creates (annihilates) an electron in site i with spin σ and $\langle i, j \rangle$ runs over nearest-neighbor sites. This Hamiltonian describes nearest-neighbor hoppings with transfer integral t , where a typical value found in the literature for this parameter is $t \sim 3.0$ eV [68]. In Appendix A, a specific expression will be given for Eq. (1) for a 3-AGNR(1,3) heterostructure, in real and reciprocal space.

In Sec. VI, long-range Coulomb interactions will be added within the DFT framework. A hybrid functional for the exchange-correlation term will be included in the DFT to better describe the Coulomb interactions as well as the Wannier-like states. The calculation methodology will be detailed in Sec. VI as well.

In the next section we will present tight-binding results for the band structure of a 3-AGNR(1,3) heterostructure. Note that the tight-binding and DFT band structures will be given in units of eV.

III. FLAT BANDS FOR A 3-AGNR(1,3) HETEROSTRUCTURE

In Fig. 2 we show the tight-binding band structure for a 3-AGNR(1,3) heterostructure, for $t = 3.00$ eV (the nearest-neighbor hopping integral value we will use for all tight-binding calculations). For the energy interval shown, we label the negative energy flat bands as 1, 2, 3a, 3b, and 4, starting from the closest one to the Fermi energy (at half-filling). Their respective energies are $E_1 = -0.56$, $E_2 = -1.61$, $E_{3a} = E_{3b} = -3.00 = -t$, and $E_4 = -4.08$ eV, where the band at $-t$ is *double degenerate*.

It is relatively well known [67] that N -AGNRs (pristine, with no extensions) with odd- N present two perfectly flat bands at $\pm t$, and Fig. 2 shows that this also happens for the 3-AGNR(1,3) heterostructure (energy $E_{3a} = E_{3b} = -t$). As a matter of fact, this is true for all odd- N N -AGNR(1,3) heterostructures we have investigated, with the difference that for $N = 3, 5$ and 7 there are additional flat bands at higher and

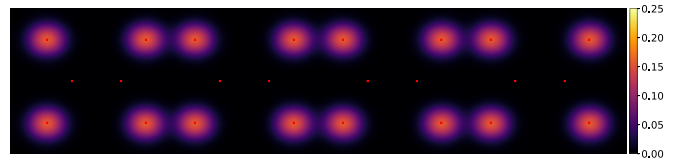


FIG. 3. Charge density of the Wannier-like state for the $-t$ flat band on a pristine 3-AGNR.

lower energies, as shown in Fig. 2. For $N \geq 9$, these additional flat bands acquire dispersion (see Sec. IV). One interesting point is that, in the N -AGNR(1,3) heterostructures, the $\pm t$ bands are double degenerate for $N = 3$ and 5 , however, this degeneracy is lifted for $N \geq 7$ (see Sec. IV).

In Ref. [67], a very interesting analysis is done of the magnetism of these $\pm t$ flat bands that are present in the odd- N AGNR (without extensions, i.e., pristine AGNR). Indeed, the origin of the zero dispersion is that the Bloch states associated with the $\pm t$ bands are formed by “isolated” clusters of charge inside each unit cell (the so-called “Wannier orbital” states, or Wannier-like states), which have *zero* overlap with the clusters in adjacent unit cells. This happens because of destructive quantum interference [67]. This phenomenon is shown in Fig. 3, which shows the integrated charge density (over all k values) for $E = -t$ in each site of an $N = 3$ pristine AGNR. Figure 3 simulates the local density of states (LDOS) an scanning tunneling microscope tip would observe in case its parameters were set to capture just the $E = -t$ states of a 3-AGNR. It is remarkable that each and every one of the different Bloch states (for different k values in the Brillouin zone) at $E = -t$ has the same LDOS profile as the one shown in Fig. 3 (see Ref. [67] for details). It is worth mentioning that these so-called Wannier-like states are also called “compact localized states” [19], which, as shown in Fig. 3, are localized on a subset of lattice sites, with zero amplitude in the rest of the lattice. As shown in the Introduction, they have recently attracted a great deal of attention. A discussion of their properties and the relevant literature may be found in Ref. [19].

Our tight-binding results for the 3-AGNR(1,3) heterostructure (Fig. 4) show that these Wannier-like $-t$ states, which exist in the odd- N pristine AGNRs, survive (basically unaffected) the (n, m) extensions that give origin to the heterostructure. This can be seen in the LDOS (charge density) profile shown in Fig. 4(c) for state E_{3a} , which shows exactly the same structure as the one in Fig. 3, with the difference that now the extended unit cell is wider, thus it accommodates four occupied dimers along the vertical direction, in contrast to the pristine 3-AGNR, where the Wannier-like state is composed of just two dimers (see Fig. 3). On the other hand, Fig. 4(d) shows the other Wannier-like state (E_{3b}) that is degenerate at $E = -t$. Interestingly, its charge profile near the edge of the extended unit cell is clearly reminiscent of the pristine 3-AGNR, while, at the center of the unit cell, it is a mixture of the E_{3a} state and some charge density occupying the maximally separated sites that are left empty by the E_{3a} state.

The interesting result shown in the other panels of Fig. 4, for the remaining three flat bands [Figs. 4(a), 4(b), and 4(e)], is that they seem to also originate from Wannier-like states with different charge configurations [when compared to Figs. 4(c)

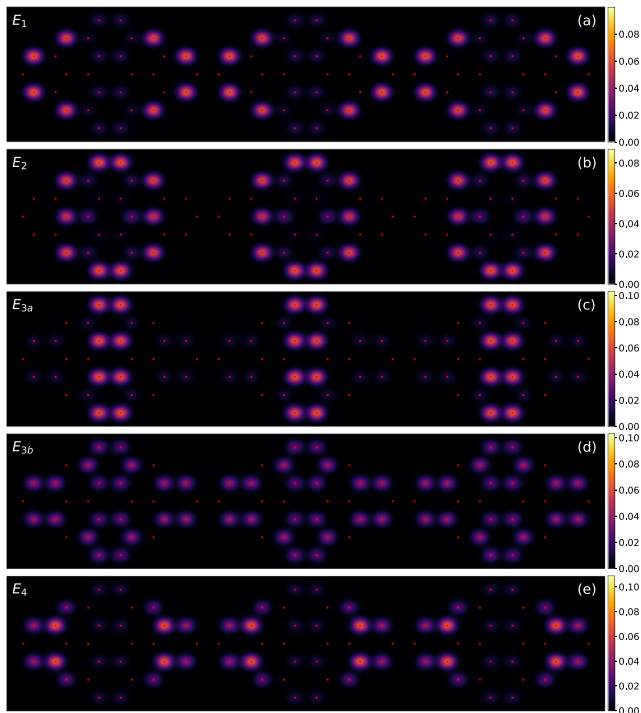


FIG. 4. Wannier-like states for all four flat bands in a 3-AGNR(1,3). From top to bottom, corresponding band energies are $E_1 = -0.56$, $E_2 = -1.61$, $E_{3a} = E_{3b} = -3.00$, and $E_4 = -4.08$ eV.

and 4(d)] that also do not have overlap between adjacent unit cells. Thus, in principle, they may produce similar magnetic ground states as the one theoretically predicted for the $\pm t$ bands in pristine N -AGNRs [67], as long as these flat bands are crossed by dispersive bands. Section VI presents a DFT analysis of this possibility.

IV. WANNIER-LIKE STATES FOR $N \geq 5$

In Figs. 5(a), 5(b), and 5(c) we see the band structure for N -AGNR(1,3) heterostructures, for $N = 5, 7$, and 9 , respectively. Despite the fact that the complexity of the band structures increases with N , we can ascertain some facts [69]: (i) flat-band 1, seen in Fig. 2, remains *perfectly* flat for $N = 5$ and 7 , although at a different energy position, while flat-band 2 has acquired a tiny dispersion; (ii) for all three values of N the $-t$ flat band is present. In reality, as far as we can tell, the $\pm t$ flat bands occur for any odd value of N ; (iii) for $N = 5$ and 7 , flat-band 4 has already acquired some dispersion; (iv) likewise, for $N \geq 9$, except for $-t$ flat band, the other three flat bands (1, 2, and 4) have acquired dispersion; (v) finally, the $-t$ flat band for $N = 5$ is still double degenerate, while it is not anymore for $N = 7$. It is possible that farther from the Fermi level ($E = 0$, at half-filling) there are additional flat bands (besides the $\pm t$ ones) for $N \geq 9$, but we have not investigated this possibility.

In Figs. 6 and 7 we show the flat-band Wannier-like states corresponding to bands 1, 2, and 3 presented in Figs. 5(a) and 5(b), for a 5-AGNR(1,3) and a 7-AGNR(1,3) heterostructure, respectively. A careful comparison of Figs. 4, 6, and 7 shows

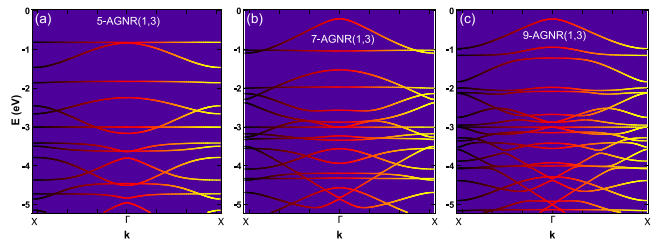


FIG. 5. Band structures for N -AGNR(1,3) heterostructures for $N = 5, 7$, and 9 in (a), (b) and (c), respectively. Although it is not so apparent, for $N = 9$ the only flat bands left is the pair $\pm t$. Aside from the $-t$ flat band, the other three flat bands in (a) and (b) have changed their positions in relation to the $N = 3$ results (see Fig. 2). Note the scale, with only negative energies, to improve readability. The band labeled 4 in (a) has acquired dispersion (compare to the corresponding band in Fig. 2.)

that the Wannier-like states for the same band at different values of N are semiquantitatively the same, indicating that the maximum N for which we can look for these interesting states is $N = 7$, which is an N -AGNR(n, m) heterostructure size that can be faithfully obtained in the laboratory [44,52,70], suggesting that the results obtained here can be tested experimentally.

As mentioned above, there is an interesting point regarding the $-t$ flat-band Wannier-like states E_{3a} and E_{3b} as we vary N in an N -AGNR(1,3) heterostructure: they are still degenerate for $N = 5$, as can be seen in Fig. 6(c), where we show the combined charge density for both bands E_{3a} and E_{3b} , however, for $N = 7$, it is not degenerate anymore. Notice that in Fig. 7(c) we show the charge density just for the E_{3a} band, since band E_{3b} does not exist anymore. We speculate that,

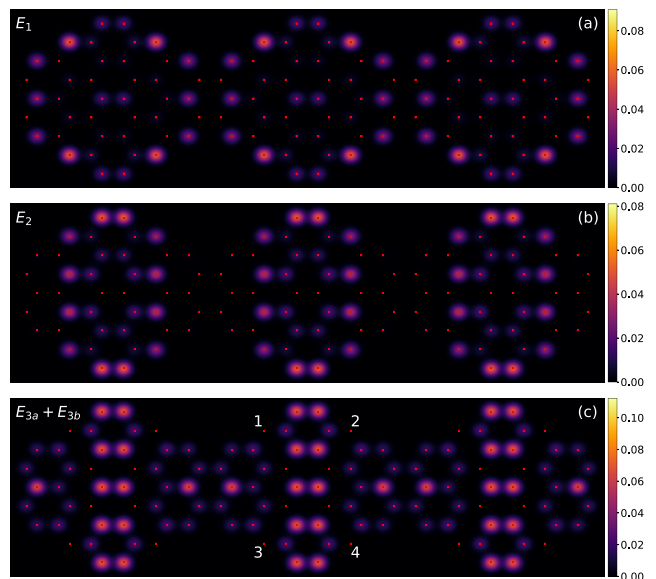


FIG. 6. Wannier-like states for three flat bands in a 5-AGNR(1,3). Numbers 1 to 4 in (c) indicate destructive quantum interference sites that prevent a continuous nearest-neighbor path from existing, which would connect all unit cells across the heterostructure, rendering state E_{3b} dispersive.

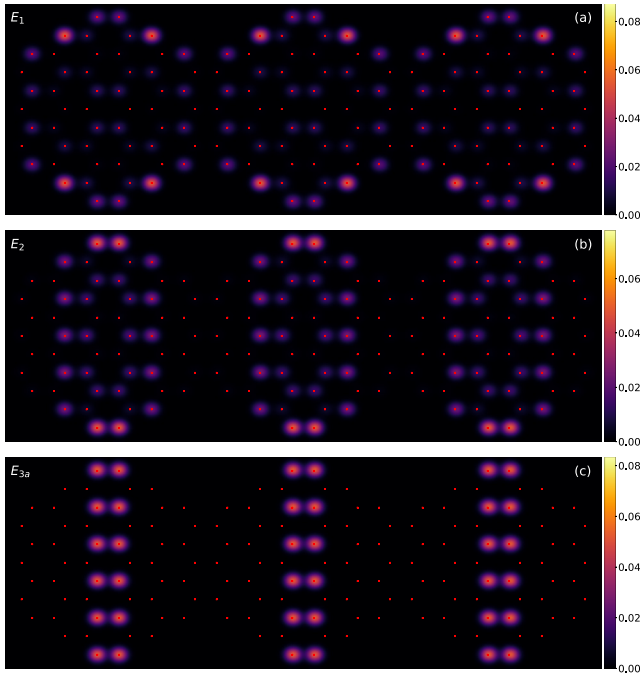


FIG. 7. Wannier-like states for three flat bands in a 7-AGNR(1,3).

as may be inferred from the charge density distribution in Fig. 6(c), the Wannier-like state E_{3a} for $N = 5$ seems on the verge of losing its Wannier-like character. This occurs because there are only 4 sites (indicated by numbers 1 to 4, and showing perfect destructive quantum interference) preventing the existence of a continuous nearest-neighbor path that connects all unit cells with each other, which would result in a dispersive state.

V. DEPENDENCE ON PARAMETERS n AND m

A. Band structure dependence with n

In Fig. 8 we see tight-binding band-structure results for 3-AGNR($n,3$), for $n = 1$ to 4, in Figs. 8(a) to 8(d), respectively. In Fig. 8(a) we repeat the results shown in Fig. 2 [for 3-AGNR(1,3)] to facilitate comparison. A trend with increasing n (size of the extended region of the heterostructure) can be clearly discerned. Indeed, we see that the $\pm t$ flat bands survive

the increase in the unit cell, and a cluster of flat bands (and some bands with very little dispersion) develops in the energy range $-2.0 \lesssim E \lesssim -1.0$. It is also interesting to remark that flat-band E_1 (the one closest to the Fermi energy) tends to approach the Fermi energy as n increases. We also did an analysis for larger values of n . For example, for $n = 10$ (not shown), bands at higher energies seem to become less dispersive. In addition, the flat band closest to the Fermi energy remains flat and approaches the Fermi energy even more, sitting basically at the Fermi energy for a 3-AGNR(10,3) heterostructure. Finally, for $n = 10$, the cluster of flat bands mentioned above becomes more dense and somewhat closer to the Fermi energy.

We also investigated the band structure dependence with n for 5-AGNR($n,3$) heterostructures (not shown) and obtained qualitatively the same results as the ones shown in Fig. 8 for $N = 3$, which may be considered reasonable, since we can intuitively expect a lesser dependence of the electronic structure on N than on n and m .

B. Band structure dependence with m

In Fig. 9 we see the band structures for 3-AGNR(1, m) heterostructures for $m = 2$ to 5 in Figs. 9(a) to 9(d), respectively. Here we also reproduced Fig. 2(b), to facilitate comparison. As seen with the variation of n (but to a lesser degree), we see in Fig. 9, for 3-AGNR(1, m), that increasing m from 2 to 5 results in an accumulation of flat bands close to the Fermi energy. In addition, as observed for the n variation, the results for the m variation of the 5-AGNR(1, m) heterostructures (not shown) are qualitatively similar to the trend seen in Fig. 9 for 3-AGNR(1, m).

We wish to call attention to the band structure in Fig. 9(a) for 3-AGNR(1,2). In it we see that the flat band closest to the Fermi energy is crossed by a dispersive band that may be topologically nontrivial [52,53]. In case this dispersive band is indeed topologically nontrivial, it would be very interesting to study the interplay of topology and ferromagnetism once this system is doped.

Before presenting the DFT results, we compile below the results presented in Figs. 4–9. This may serve as a guide to the reader to relate the presence (or absence) and behavior of flat bands with the variation of parameters N , n , and m :

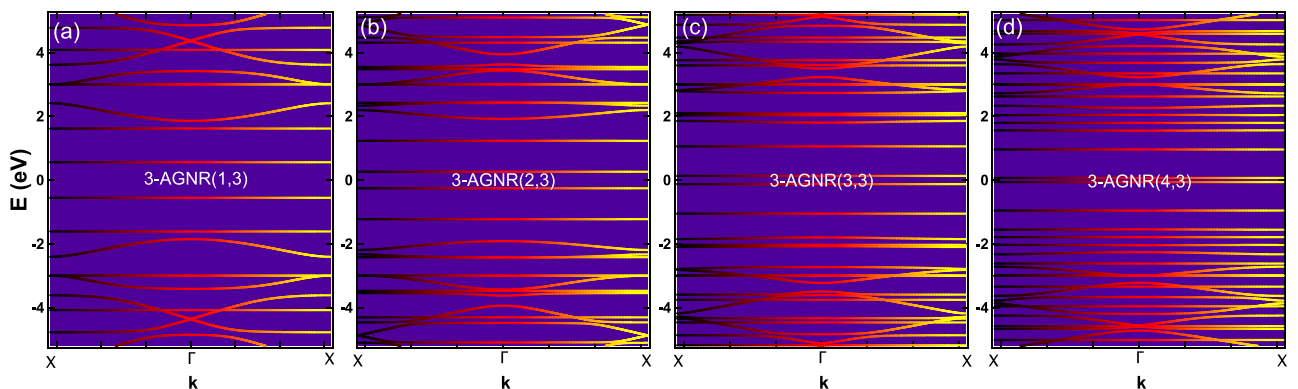


FIG. 8. Band structures for 3-AGNR($n,3$) heterostructures for $n = 1$ to 4, in (a) to (d), respectively.

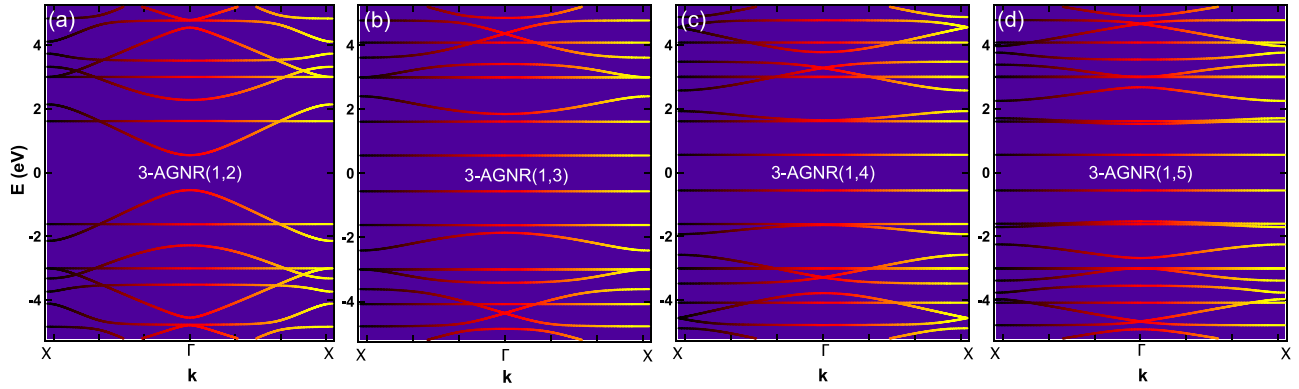


FIG. 9. Band structures for 3-AGNR(1, m) heterostructures for $m = 2$ to 5, in (a) to (d), respectively.

(1) The $\pm t$ flat bands, present in the pristine AGNRs, are also present for *all* values of N , n , and m investigated here, and they are associated with the *same* Wannier-like states identified in the pristine AGNRs [67].

(2) For N -AGNR(1,3) ($N = 3$ and 5), the $\pm t$ bands are double degenerate (in contrast to the pristine AGNRs) and the partner state is also a Wannier-like state, similar to the one mentioned in the item above. This degeneracy is lifted for $N > 5$.

(3) Additional flat bands appear around the $\pm t$ flat bands for all heterostructures analyzed, and to each different flat band it was possible to associate a Wannier-like state that seems like a variant of the $\pm t$ Wannier-like state.

(4) Regarding the variation of these additional flat bands with N , we see that they survive (i.e., have zero dispersion) up to $N = 7$ for all heterostructures studied here.

(5) With increasing n , we see that the overall number of flat bands increases, with a cluster of them forming gradually closer to the Fermi energy, with one of them seating almost *at* the Fermi energy already for the 3-AGNR(10,3) heterostructure. This description of the n dependence applies to all prime values $3 \leq N \leq 7$.

(6) Similar to the n dependence, there is an increase in the number of flat bands with m , with a similar accumulation close to the Fermi energy. As well, this description qualitatively applies to all prime values $3 \leq N \leq 7$.

We should also mention that a brief study of the so-called “staggered” heterostructures, which are less symmetric than the ones analyzed here (see Refs. [52,53]), has shown a tendency to form considerably less flat bands, indicating that the heterostructures discussed here are the ones that should receive more attention in the quest for quasi-1D ferromagnetism.

VI. FERROMAGNETIC PHASE OBTAINED WITH DFT

To address the possible existence of any magnetic phase under hole doping, we will use DFT, which is a more realistic calculation than tight binding and that can treat correlations at the mean-field level. We will search for indications of a ferromagnetic ground state on two heterostructures, viz., 3-AGNR(1,3) and 5-AGNR(1,3). According to Ref. [67], the

presence of itinerant carriers is important to mediate ferromagnetism between the isolated magnetic moments in each unit cell of the Wannier-like states. The 3-AGNR(1,3) and 5-AGNR(1,3) heterostructures present dispersive bands intercepting the flat bands, as can be seen in Figs. 2 and 5(a), respectively. We will postpone a careful DFT analysis of the ferromagnetic ground-state dependence on the parameters n and m to a future publication.

A. Details of the DFT calculations

We do a DFT calculation within the projector augmented wave scheme [71] for the pseudopotentials. The total energies and electronic structures are self-consistently computed within a plane-wave basis set with a kinetic energy cutoff of 350 eV. We used the Vienna *ab initio* simulation package (VASP) [72,73]. For a better description of the exchange-correlation term of the DFT, we use a hybrid functional to improve the description of the many-electron interactions and charge localization [74]. The HSE06 hybrid functional has been used [75], where the screened functional contains part of the exact Hartree-Fock exchange that has been shown to give accurate results for the exchange splitting, which is crucial to understand the magnetic properties in our system. Interestingly, our results show that the inclusion of the hybrid functional puts the E_{3a} flat band around 3 eV from the Fermi energy, matching the tight-binding results (see Fig. 10). By suppressing the hybrid functional, using just the generalized gradient approximation [76], the E_{3a} band stays around 2.5 eV from the Fermi level. As we are using the periodic supercell approach within the first-principles calculations, the exchange interactions between adjacent unit cells are also included.

B. Band structure for 3-AGNR(1,3): Comparison DFT/tight binding

Figures 10(a) and 10(b) show a comparison of the DFT and tight-binding band structures for a 3-AGNR(1,3) heterostructure, respectively. Contrary to the tight-binding bands, the DFT bands are not mirror symmetric around $E = 0$. Note that the tight-binding bands would also lack mirror symmetry if a next-nearest-neighbor hopping had been introduced (breaking chiral symmetry). Some details of the negative energy DFT

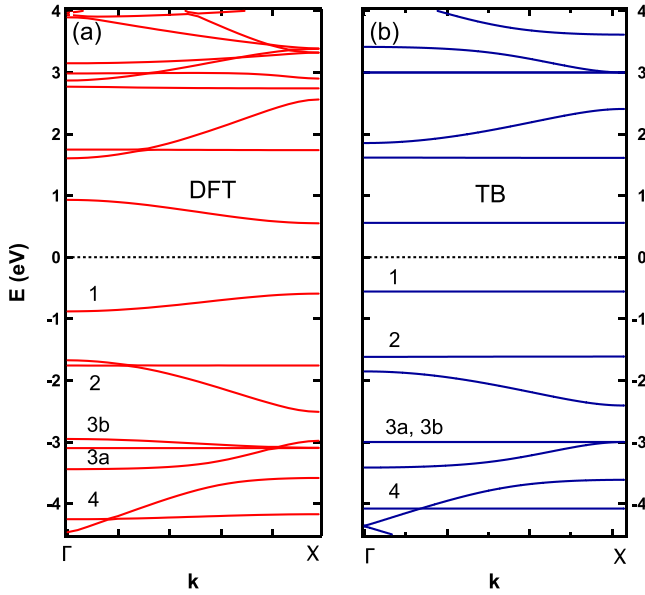


FIG. 10. DFT and tight-binding band structures for a 3-AGNR(1,3) heterostructure, at half-filling, in (a) and (b), respectively. As expected, the DFT bands are not particle-hole symmetric, but, other than that, there is a good qualitative agreement between DFT and tight binding. The numbered bands are discussed in the text.

bands are worthy of mention. First, we see that the DFT band closest to the Fermi energy (numbered 1 in Fig. 10), which is flat in the tight-binding results, has acquired dispersion. Figure 4(a) shows the tight-binding Wannier-like state for this band. Since its charge density is mostly accumulated at the edges of the unit cell (and it does not completely vanish at its center either), one may argue that small perturbations introduced by the DFT calculations to the tight-binding results may create an overlap between the Wannier-like states in adjacent unit cells and result in dispersion [as discussed above in relation to the E_{3b} tight-binding band for a 5-AGNR(1,3) heterostructure]. On the other hand, the Wannier-like states [see Figs. 4(b) and 4(c)] for the bands denoted 2 and 3a in Fig. 10 are much more concentrated at the center of the unit cell [especially for band 3a, see Fig. 4(c)] and thus they should be more robust against perturbations that could create an overlap between adjacent unit cells. Thus, as expected, DFT bands 2 and 3a are *perfectly* flat. Finally, the same reasoning leads us to expect that the DFT bands 3b and 4 should acquire dispersion, as they do indeed, the latter less so than the former.

A final point can be made, along the lines of the qualitative discussion above, if we compare our DFT results with the DFT results in Ref. [67]. There, it was obtained, for a pristine (no extensions) 5-AGNR, that the $\pm t$ DFT flat bands, at zero doping, acquire a dispersion of ≈ 0.4 eV (see Fig. 4(a) in Ref. [67]). On the other hand, the DFT $\pm t$ bands for N -AGNR(1,3), for $N = 3$ [band 3a in Fig. 10(a)] and $N = 5$ (not shown), are *perfectly* flat. This seems to indicate that in an N -AGNR(n, m) heterostructure, which has a wider unit cell than a pristine AGNR, the charge density of the $\pm t$ Wannier-like states in each unit cell [like the ones shown in Figs. 4(c), 6(c), and 7(c)] is even more insulated from the charge density in

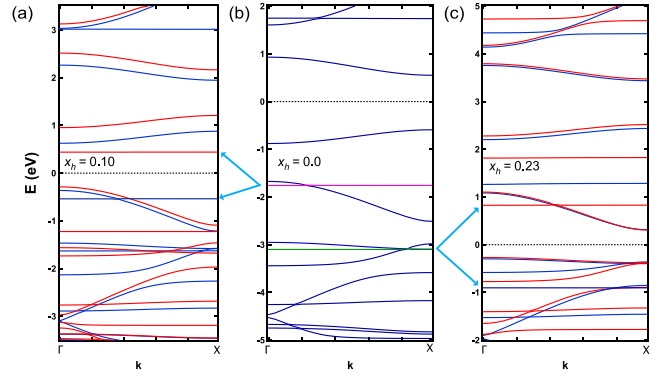


FIG. 11. DFT band structures for a 3-AGNR(1,3) heterostructure at different hole dopings: (a) $x_h = 0.10$, (b) $x_h = 0.0$ (half-filling), and (c) $x_h = 0.23$. In (a) and (c), majority-spin bands are in blue and minority-spin bands are in red.

adjacent unit cells, and thus can result in a more robust (more massive) DFT flat band.

C. DFT bands at finite doping and ferromagnetic ground state

To bring the Fermi energy close to the flat bands, and thus investigate their properties, we start hole doping the 3-AGNR(1,3) heterostructure. We measure the hole doping x_h from the half-filling point, thus $x_h = 1 - \langle n \rangle$ (therefore, $x_h = 0$ at half-filling), where $\langle n \rangle$ is the electron average site occupancy.

In Fig. 11 we show the DFT bands for $x_h = 0.10$, 0.0 (half-filling), and 0.23, in Figs. 11(a) to 11(c), respectively. The Fermi energy is at $E = 0.0$ in each panel. In Fig. 11(b) we repeat the results shown in Fig. 10(a) to better illustrate the hole-doping effects. In Figs. 11(a) and 11(c), at finite doping, we show the spin-decomposed band structure obtained through a hybrid DFT calculation, where the majority-spin bands are denoted in blue and the minority-spin bands are in red. The cyan arrows connecting the center panel to each one of the adjacent panels indicate the extent of the exchange splitting of each flat band. The arrows connecting band 2 [in Fig. 11(b)] to the corresponding exchange-split bands in Fig. 11(a) indicate the extent of the exchange splitting energy acting over band 2 for $x_h = 0.1$, given by $E_{2,0.1} \approx 1.0$ eV.

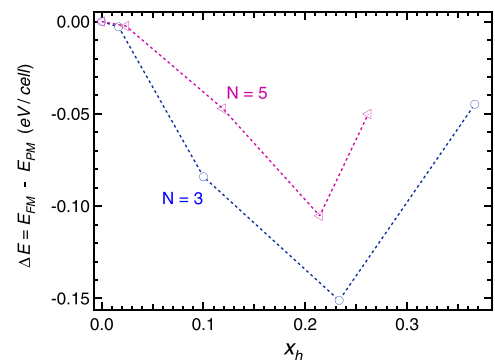


FIG. 12. $\Delta E = E_{FM} - E_{PM}$ as a function of hole doping x_h for 3-AGNR(1,3) (blue circles) and 5-AGNR(1,3) (purple left triangles).

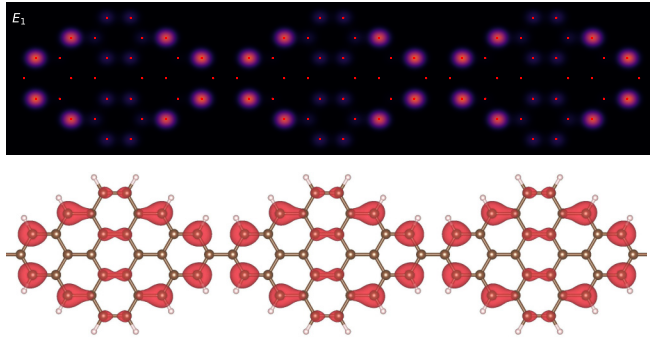


FIG. 13. Wannier-like state for flat-band E_1 for a 3-AGNR(1,3) heterostructure. Top panel: Tight-binding result; bottom panel: DFT result.

Likewise, the arrows connecting Figs. 11(b) and 11(c) indicate the exchange splitting energy of band 3a for $x_h = 0.23$, corresponding to $E_{3a,0.23} \approx 2.0$ eV.

In Fig. 12 we show the energy difference between the ferromagnetic and paramagnetic states, $\Delta E = E_{\text{FM}} - E_{\text{PM}}$, for both a 3-AGNR(1,3) (blue circles) and a 5-AGNR(1,3) (purple left triangles), where $\Delta E < 0$ indicates a ferromagnetic ground state. The most stable ferromagnetic configuration occurs when the hole doping reaches the 3a flat band, for both 3- and 5-AGNR(1,3). The inverse dependence of the ferromagnetic stability with N can be attributed to the reduction of the overall band flatness as N increases (see Figs. 2 and 5).

From Ref. [67] we obtain that the gain in energy due to ferromagnetic ordering of a pristine 5-AGNR is $\Delta E_p \approx -37.5$ meV (per unit cell). Since the number of occupied carbon atoms in the ferromagnetic state in each unit cell is $N_{\text{occ}} = 6$ (see Fig. 5(b) in Ref. [67]), we obtain $\frac{\Delta E_p}{N_{\text{occ}}} = -6.25$ meV. The corresponding results for the two heterostructures we analyzed through DFT, i.e., 3-AGNR(1,3) and 5-AGNR(1,3), were $\Delta E_3 = -150$ meV, $N_{\text{occ}} = 8$ and $\Delta E_5 = -105$ meV, $N_{\text{occ}} = 10$. This results in $\frac{\Delta E_N}{N_{\text{occ}}} = -18.8$ and -10.5 meV, respectively. This shows that, if we compare the ferromagnetic energy gain for the pristine 5-AGNR and the 5-AGNR(1,3), the heterostructure had almost 70% more energy gain than that of the pristine AGNR. We believe that to be the case for two main reasons. First, the N -AGNR(n, m) heterostructures studied here through DFT present true flat bands, contrary to what was seen in the pristine N -AGNRs studied in Ref. [67]. Second, the pristine N -AGNRs show a single *low-dispersion* band, while our N -AGNR(n, m) heterostructures show multiple *perfectly* flat bands [two in the case of 3-AGNR(1,3), bands labeled 2 and 3a in Fig. 10(a)] and multiple *almost* flat bands [two in the case of 3-AGNR(1,3), bands 3b and 4 in Fig. 10(a)], which should clearly result in a more robust ferromagnetic ground state.

VII. WANNIER-LIKE STATES: COMPARISON BETWEEN DFT AND TIGHT BINDING

In this section we want to highlight the fact that it is not only the DFT and tight-binding band structures that are qualitatively similar (as shown in Fig. 10), but also the Wannier-like states associated with the flat bands obtained by either method that are qualitatively similar too.

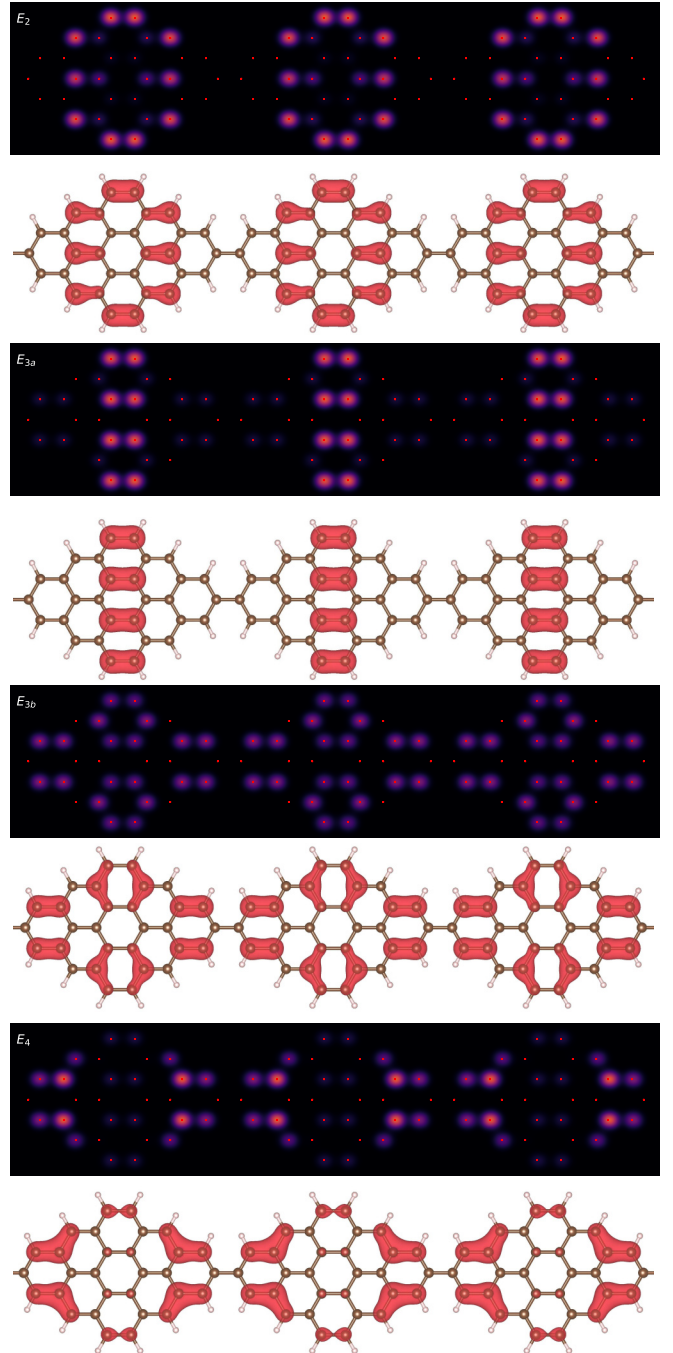


FIG. 14. Wannier-like states for flat bands E_2 , E_{3a} , E_{3b} , and E_4 for a 3-AGNR(1,3) heterostructure. Top panel: Tight-binding result; bottom panel: DFT result, for all pairs of results.

In the top panel of Fig. 13 we reproduce Fig. 4(a), with the tight-binding result for the flat-band E_1 Wannier-like state for a 3-AGNR(1,3) at half-filling. In the bottom panel we show the corresponding DFT result. Close inspection indicates that there is a semiquantitative agreement between tight binding and DFT. Figure 14 makes the same comparison for flat bands 2, 3a, 3b, and 4, and close inspection of the plots shows that the tight-binding results are surprisingly close to the DFT results in all cases.

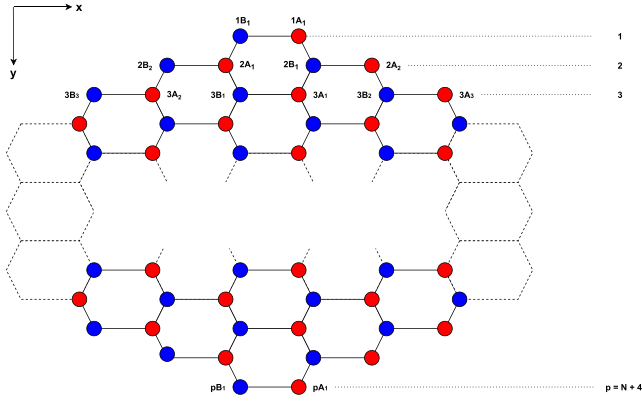


FIG. 15. Site labeling of a unit cell for an N -AGNR(1,3) heterostructure. The sites are labeled $p\alpha_q$, where $\alpha = A/B$, $1 \leq p \leq N + 4$, and $1 \leq q \leq 3$, see text for details.

VIII. SUMMARY AND CONCLUSIONS

We have used the tight-binding and DFT methods to study the electronic properties of recently synthesized N -AGNR(n, m) graphene heterostructures [52,53], which have been shown to present, for specific values of N , n , and m , topological properties at low energy that can be simulated by the SSH model. We found out that the heterostructures show a multiplicity of flat bands, whose properties can be reasonably well controlled by the parameters N , n , and m . We see flat bands in our heterostructures up to $N = 7$. We have strong indications that the quantum interference mechanism that gives origin to the $\pm t$ single flat band in pristine AGNRs [67] is at play in all the flat bands analyzed in our heterostructures. The pristine AGNR $\pm t$ bands are still present in the heterostructures, but with the interesting presence of a degenerate partner (for $N = 3$ and 5) in the tight-binding simulations. This degeneracy is slightly lifted in the DFT results for all values of N . Importantly, our DFT results show that a few of the flat bands observed in the tight-binding simulations remain *perfectly* flat in the DFT simulations as

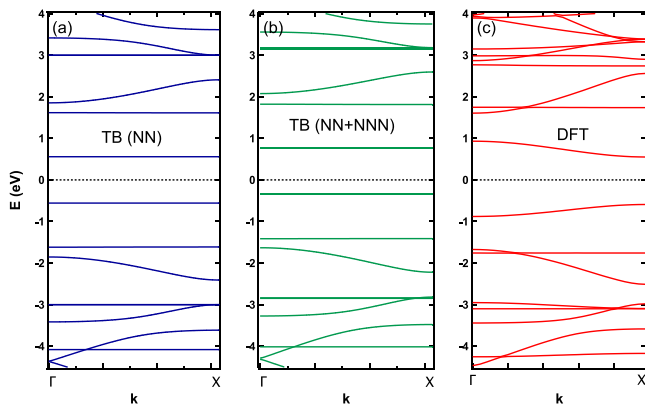


FIG. 16. (a) Tight-binding band structure for 3-AGNR(1,3) with NN hoppings only [reproduced from Fig. 10(b)]. (b) Same as in (a), but adding a NNN hopping t_{NNN} to the calculations, with $t_{\text{NNN}} = 0.1$ eV [68]. (c) DFT results for 3-AGNR(1,3) [reproduced from Fig. 10(a)].

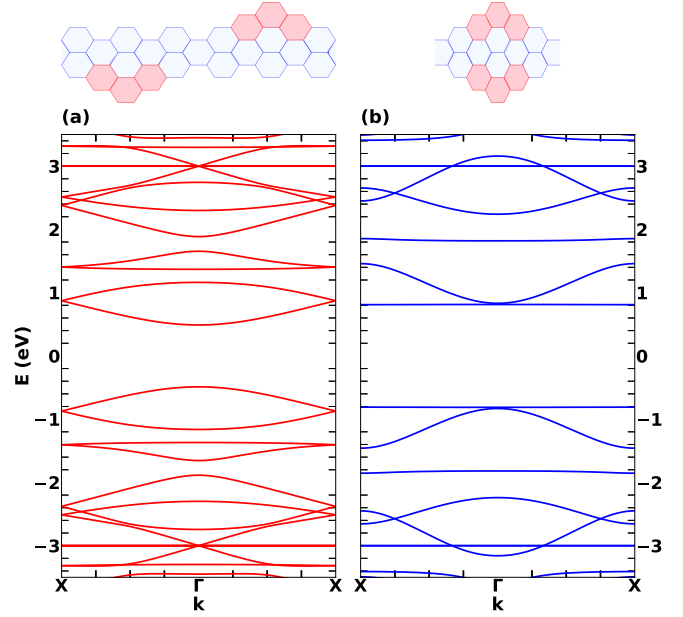


FIG. 17. (a) Tight-binding band structure for 5-AGNR-S(1,3). (b) Tight-binding band structure for 5-AGNR(1,3). The unit cell of each heterostructure is shown at the top of each panel.

well. Thus, the ferromagnetism observed in our DFT results is considerably stronger than that observed in pristine AGNRs [67]. As a bonus, we found that the charge density associated with the flat bands obtained via tight binding agree surprisingly well with the corresponding results obtained through DFT.

Given the experimental availability of these heterostructures, our results suggest that it would be interesting to

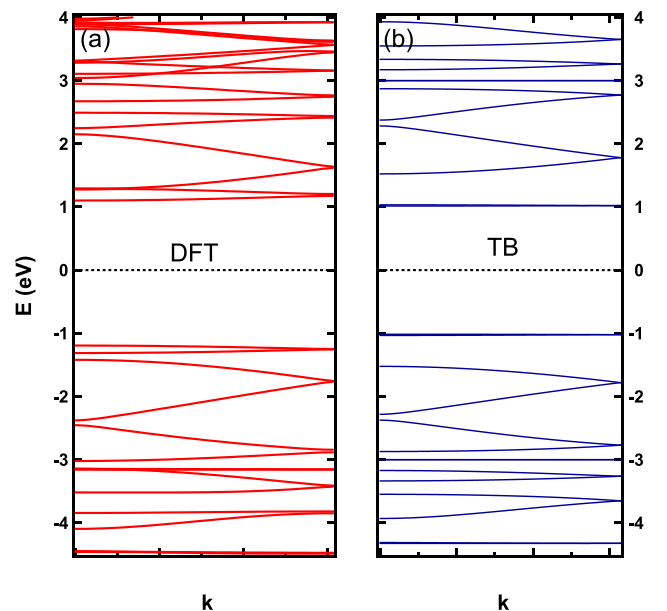


FIG. 18. (a) DFT band structure for 3-AGNR-S(1,3). (b) Tight-binding band structure for 3-AGNR-S(1,3).

experimentally explore the possibility of ferromagnetism in these systems, which, given the variety of parameters that can be manipulated, opens up the possibility of looking for nontrivial topology in a ferromagnetic quasi-1D system.

ACKNOWLEDGMENTS

P.A.A. thanks the Brazilian funding agency CAPES for financial support. T.M.S. acknowledges INCT in Carbon Nanomaterials, CNPq, FAPEMIG, and the computational facilities from LNCC and Cenapad. G.B.M. acknowledges financial support from the Brazilian agency Conselho Nacional de Desenvolvimento Científico e Tecnológico (CNPq), processes 424711/2018-4, 305150/2017-0, and 210355/2018.

APPENDIX A: TIGHT-BINDING HAMILTONIAN FOR AN N -AGNR(1,3) HETEROSTRUCTURE

In this Appendix we present explicit expressions for the Hamiltonian of an N -AGNR(1,3) heterostructure, in real and reciprocal spaces. The modifications necessary to obtain the Hamiltonian for a general N -AGNR(n, m) heterostructure are straightforward. In Fig. 15 we show the l th unit cell of an N -AGNR(1,3) heterostructure, where the A sublattice is represented by blue solid dots and the B sublattice by red solid dots. The sites are labeled $p\alpha_q$, where $\alpha = A/B$, with $1 \leq p \leq N+4$ and $1 \leq q \leq 3$, where p runs along the y direction, as indicated on the right-hand side, and q runs along the x direction (starting at the center of the unit cell and moving to its borders).

Using the labeling defined above, we can write the N -AGNR(1,3) Hamiltonian in real space as

$$\begin{aligned}
 H = & -t \sum_l \left[\sum_{p \in \text{odd}}^N b_{l,1}^\dagger(p) a_{l,1}(p) + \sum_{p=2}^{N-1} b_{l,1}^\dagger(p+1) a_{l,1}(p) + \sum_{p=2}^{N-1} a_{l,1}^\dagger(p+1) b_{l,1}(p) + \text{H.c.} \right] \\
 & - t \sum_l \left[\sum_{p=2}^{N-2} b_{l,2}^\dagger(p+1) a_{l,2}(p) + \sum_{p=2}^{N-2} a_{l,2}^\dagger(p+1) b_{l,2}(p) + \text{H.c.} \right] \\
 & - t \sum_l \left[\sum_{\substack{p=2 \\ m \in \text{even}}}^{N-1} b_{l,1}^\dagger(p) a_{l,2}(p) + \sum_{\substack{p=2 \\ m \in \text{even}}}^{N-1} b_{l,2}^\dagger(p) a_{l,1}(p) + \text{H.c.} \right] \\
 & - t \sum_l \left[\sum_{p=3}^{N-3} b_{l,3}^\dagger(p+1) a_{l,3}(p) + \sum_{p=3}^{N-3} a_{l,3}^\dagger(p+1) b_{l,3}(p) + \text{H.c.} \right] \\
 & - t \sum_l \left[\sum_{\substack{p=3 \\ m \in \text{odd}}}^{N-2} b_{l,2}^\dagger(p) a_{l,3}(p+1) + \sum_{\substack{p=3 \\ m \in \text{odd}}}^{N-2} b_{l,3}^\dagger(p+1) a_{l,2}(p) + \sum_{\substack{p=4 \\ m \in \text{even}}}^{N-3} b_{l-1,3}^\dagger(p) a_{l,3}(p) + \text{H.c.} \right], \quad (\text{A1})
 \end{aligned}$$

where $a_{l,q}(p)$ [$b_{l,q}(p)$] annihilates an electron on site pA_q (pB_q) on the l th unit cell. Assuming periodic boundary conditions along the x direction, we take a Fourier transform along that direction and obtain the reciprocal space Hamiltonian

$$\begin{aligned}
 H = & -t \sum_k \left[\sum_{m \in \text{odd}}^N v_1 \beta_{k,1}^\dagger(p) \alpha_{k,1}(p) + \sum_{p=2}^{N-1} v_2 \beta_{k,1}^\dagger(p+1) \alpha_{k,1}(p) + \sum_{p=2}^{N-1} v_3 \alpha_{k,1}^\dagger(p+1) \beta_{k,1}(p) + \text{H.c.} \right] \\
 & - t \sum_k \left[\sum_{p=2}^{N-2} v_2 \beta_{k,2}^\dagger(p+1) \alpha_{k,2}(p) + \sum_{p=2}^{N-2} v_3 \alpha_{k,2}^\dagger(p+1) \beta_{k,2}(p) + \text{H.c.} \right] \\
 & - t \sum_k \left[\sum_{\substack{p=2 \\ m \in \text{even}}}^{N-1} v_1 \beta_{k,1}^\dagger(p) \alpha_{k,2}(p) + \sum_{\substack{p=2 \\ m \in \text{even}}}^{N-1} v_1 \beta_{k,2}^\dagger(p) \alpha_{k,1}(p) + \text{H.c.} \right] \\
 & - t \sum_k \left[\sum_{p=3}^{N-3} v_1 \beta_{k,3}^\dagger(p+1) \alpha_{k,3}(p) + \sum_{p=3}^{N-3} v_1 \alpha_{k,3}^\dagger(p+1) \beta_{k,3}(p) + \text{H.c.} \right] \\
 & - t \sum_k \left[\sum_{\substack{p=3 \\ m \in \text{odd}}}^{N-2} v_2 \beta_{k,2}^\dagger(p) \alpha_{k,3}(p+1) + \sum_{\substack{p=3 \\ m \in \text{odd}}}^{N-2} v_3 \beta_{k,3}^\dagger(p+1) \alpha_{k,2}(p) + \sum_{\substack{p=4 \\ m \in \text{even}}}^{N-3} v_1 \beta_{k,3}^\dagger(p) \alpha_{k,3}(p) + \text{H.c.} \right], \quad (\text{A2})
 \end{aligned}$$

where $\alpha_{k,q}(p)$ and $\beta_{k,q}(p)$ are the Fourier transformed operators, and $v_1 = e^{-ika_T/9}$, $v_2 = e^{ika_T/18}$, and $v_3 = e^{-ika_T/18}$, with $a_T = 1$ the unit cell size.

APPENDIX B: TIGHT BINDING WITH NEXT-NEAREST-NEIGHBOR HOPPING

In Fig. 16 we present tight-binding and DFT results to assess the stability of the tight-binding flat bands to the addition of a NNN hopping t_{NNN} to the calculations. In Fig. 16(a) we reproduce the tight-binding bands shown previously in Fig. 10(b) for 3-AGNR(1,3), which included just nearest-neighbor (NN) hoppings. In Fig. 16(b) we add NNN hoppings $t_{\text{NNN}} = 0.1$ eV [68] to the calculations. As expected, the results are not particle-hole symmetric anymore. However, all the flat bands (in the interval of energy shown) remain flat. Thus, since the DFT results [in Fig. 16(c), reproduced from Fig. 10(a)] show that flat-band 1 (the closest to the Fermi energy) has acquired dispersion, we conclude that longer hoppings than NNN are necessary in the tight-binding calculations to produce dispersion in flat-band 1. This can be understood by looking at the Wannier-like state for this band, shown in Fig. 4(a). There we clearly see that, to connect two unit cells, it is necessary at least a third NN hopping. This may explain too why flat-band 3b has acquired a small dispersion, while flat-band 4 has acquired just a slight dispersion.

APPENDIX C: RESULTS FOR STAGGERED HETEROSTRUCTURES

In Refs. [52,53] a second type of heterostructure has been introduced, less symmetric than the one we analyzed in this work. The reason we did not focus our attention in these so-called staggered heterostructures is that they show less

flat bands than the so-called inline heterostructures (which were the focus of this work). To exemplify that, in Fig. 17(a) we compare the tight-binding band structure results for a 5-AGNR-S(1,3) heterostructure [Fig. 17(a)] with that for a 5-AGNR-(1,3) one [Fig. 17(b)]. Notice the inclusion of an “S” (in bold, for staggered) to the label for the heterostructure. On top of Fig. 17(a) we show a single unit cell for the 5-AGNR-S(1,3) heterostructure. By comparing it to the single unit cell on top of Fig. 17(b) [for 5-AGNR-(1,3)], which was described in Sec. II A, it is easy to understand the meaning of the (1,3) nomenclature, since the idea is the same as the one introduced in Sec. II A.

By comparing the two panels, one notices that only the $\pm t$ flat bands have survived in the staggered heterostructure. We have checked that what appears to be two flat bands (touched by a dispersive band, located, respectively, between energies -1 and -2 eV, and below energy -3 eV) are in reality two slightly dispersive bands, and not perfectly flat, like the $\pm t$ flat bands. Our conclusion also rests in the fact that we could not discern a clear Wannier-like state associated with them. Thus, in the 5-AGNR-S(1,3) heterostructure there are just 1/4 of the flat bands present in the (inline) 5-AGNR(1,3) heterostructure, shown in Fig. 17(b).

Finally, for completeness sake, in Fig. 18 we show a comparison of the DFT band structure for 3-AGNR-S(1,3), with the tight-binding band structure, in Figs. 18(a) and 18(b), respectively. Aside from the expected broken particle-hole symmetry in the DFT bands, it is easy to see the very good agreement between the two results. A careful analysis of the DFT results shows that the only flat band that is perfectly nondispersive is the $\pm t$ flat band (located just below -3 eV), reinforcing our claim that the inline heterostructures have more robust flat bands.

-
- [1] Y. Cao, V. Fatemi, A. Demir, S. Fang, S. L. Tomarken, J. Y. Luo, J. D. Sanchez-Yamagishi, K. Watanabe, T. Taniguchi, E. Kaxiras, R. C. Ashoori, and P. Jarillo-Herrero, *Nature (London)* **556**, 80 (2018).
 - [2] E. Y. Andrei and A. H. MacDonald, *Nat. Mater.* **19**, 1265 (2020).
 - [3] J. M. B. Lopes dos Santos, N. M. R. Peres, and A. H. Castro Neto, *Phys. Rev. Lett.* **99**, 256802 (2007).
 - [4] E. Suárez Morell, J. D. Correa, P. Vargas, M. Pacheco, and Z. Barticevic, *Phys. Rev. B* **82**, 121407(R) (2010).
 - [5] R. Bistritzer and A. H. MacDonald, *Proc. Natl. Acad. Sci. USA* **108**, 12233 (2011).
 - [6] S. Lisi, X. Lu, T. Benschop, T. A. de Jong, P. Stepanov, J. R. Duran, F. Margot, I. Cucchi, E. Cappelli, A. Hunter, A. Tamai, V. Kandyba, A. Giampietri, A. Barinov, J. Jobst, V. Stalman, M. Leeuwenhoek, K. Watanabe, T. Taniguchi, L. Rademaker *et al.*, *Nat. Phys.* **17**, 189 (2021).
 - [7] M. N. Huda, S. Kezilebieke, and P. Liljeroth, *Phys. Rev. Research* **2**, 043426 (2020).
 - [8] H. Liu, Y. Cao, Y. Xu, D. J. Gawryluk, E. Pomjakushina, S.-Y. Gao, P. Dudin, M. Shi, L. Yan, Y.-f. Yang, and H. Ding, *Phys. Rev. B* **102**, 035111 (2020).
 - [9] L. S. G. Leite and R. L. Doretto, *Phys. Rev. B* **104**, 155129 (2021).
 - [10] S. M. Chan, B. Grémaud, and G. G. Batrouni, *Phys. Rev. B* **105**, 024502 (2022).
 - [11] T. Orito, Y. Kuno, and I. Ichinose, *Phys. Rev. B* **104**, 094202 (2021).
 - [12] J. Richter, V. Ohanyan, J. Schulenburg, and J. Schnack, *arXiv:2107.04371*.
 - [13] P. Kumar, G. Chen, and J. L. Lado, *Phys. Rev. Research* **3**, 043113 (2021).
 - [14] T. Cadez, Y. Kim, A. Andreanov, and S. Flach, *Phys. Rev. B* **104**, L180201 (2021).
 - [15] T. Mizoguchi, Y. Kuno, and Y. Hatsugai, *arXiv:2108.02414*.
 - [16] K. T. K. Chung, J. S. K. Goh, A. Mukherjee, W. Jin, D. Lozano-Gómez, and M. J. P. Gingras, *arXiv:2108.07816*.
 - [17] W. R. Meier, M.-H. Du, S. Okamoto, N. Mohanta, A. F. May, M. A. McGuire, C. A. Bridges, G. D. Samolyuk, and B. C. Sales, *Phys. Rev. B* **102**, 075148 (2020).
 - [18] L. Ye, S. Fang, M. G. Kang, J. Kaufmann, Y. Lee, J. Denlinger, C. Jozwiak, A. Bostwick, E. Rotenberg, E. Kaxiras, D. C. Bell, O. Janson, R. Comin, and J. G. Checkelsky, *arXiv:2106.10824*.
 - [19] C. V. Morfonios, M. Röntgen, M. Pyzh, and P. Schmelcher, *Phys. Rev. B* **104**, 035105 (2021).

- [20] J.-W. Rhim and B.-J. Yang, *Phys. Rev. B* **99**, 045107 (2019).
- [21] Y. Hwang, J.-W. Rhim, and B.-J. Yang, *Phys. Rev. B* **104**, L081104 (2021).
- [22] N. Grandi, V. Juricic, I. S. Landea, and R. Soto-Garrido, *J. High Energy Phys.* **05** (2021) 123.
- [23] H. Nakai and C. Hotta, [arXiv:2103.13672](https://arxiv.org/abs/2103.13672).
- [24] T. Mizoguchi, H. Katsura, I. Maruyama, and Y. Hatsugai, *Phys. Rev. B* **104**, 035155 (2021).
- [25] Y. Hatsugai, *Ann. Phys.* **435**, 168453 (2021).
- [26] J. Wang, J. Cano, A. J. Millis, Z. Liu, and B. Yang, *Phys. Rev. Lett.* **127**, 246403 (2021).
- [27] J. Zurita, C. Creffield, and G. Platero, *Quantum* **5**, 591 (2021).
- [28] A. Kruchkov, [arXiv:2105.14672](https://arxiv.org/abs/2105.14672).
- [29] Z. Liu, H. Wang, and J. Wang, [arXiv:2106.01630](https://arxiv.org/abs/2106.01630).
- [30] D. Calugaru, A. Chew, L. Elcoro, N. Regnault, Z.-D. Song, and B. A. Bernevig, *Nat. Phys.* **18**, 185 (2022).
- [31] A. Luo, Z. Song, and G. Xu, [arXiv:2107.05433](https://arxiv.org/abs/2107.05433).
- [32] A. Graf and F. Piéchon, *Phys. Rev. B* **104**, 195128 (2021).
- [33] S. Li, Y. Xie, and Y. Chen, *Phys. Rev. B* **104**, 085127 (2021).
- [34] C. Bao, H. Zhang, X. Wu, S. Zhou, Q. Li, P. Yu, J. Li, W. Duan, and S. Zhou, [arXiv:2108.07254](https://arxiv.org/abs/2108.07254).
- [35] J. Wang and Z. Liu, [arXiv:2109.10325](https://arxiv.org/abs/2109.10325).
- [36] S. Pathak, T. Rakib, R. Hou, A. Nevidomskyy, E. Ertekin, H. T. Johnson, and L. K. Wagner, [arXiv:2110.03508](https://arxiv.org/abs/2110.03508).
- [37] M. S. M. de Sousa, F. Liu, F. Qu, and W. Chen, *Phys. Rev. B* **105**, 014511 (2021).
- [38] B. Sutherland, *Phys. Rev. B* **34**, 5208 (1986).
- [39] E. H. Lieb, *Phys. Rev. Lett.* **62**, 1201 (1989).
- [40] S. A. Parameswaran, R. Roy, and S. L. Sondhi, *C. R. Phys.* **14**, 816 (2013).
- [41] E. J. Bergholtz and Z. Liu, *Int. J. Mod. Phys. B* **27**, 1330017 (2013).
- [42] D. Leykam, A. Andreanov, and S. Flach, *Adv. Phys.: X* **3**, 1473052 (2018).
- [43] O. Derzhko, J. Richter, and M. Maksymenko, *Int. J. Mod. Phys. B* **29**, 1530007 (2015).
- [44] J. Cai, P. Ruffieux, R. Jaafar, M. Bieri, T. Braun, S. Blankenburg, M. Muoth, A. P. Seitsonen, M. Saleh, X. Feng, K. Muellen, and R. Fasel, *Nature (London)* **466**, 470 (2010).
- [45] T. Cao, F. Zhao, and S. G. Louie, *Phys. Rev. Lett.* **119**, 076401 (2017).
- [46] M. König, H. Buhmann, L. W. Molenkamp, T. Hughes, C.-X. Liu, X.-L. Qi, and S.-C. Zhang, *J. Phys. Soc. Jpn.* **77**, 031007 (2008).
- [47] M. Z. Hasan and C. L. Kane, *Rev. Mod. Phys.* **82**, 3045 (2010).
- [48] X.-L. Qi and S.-C. Zhang, *Rev. Mod. Phys.* **83**, 1057 (2011).
- [49] B. Yan and S.-C. Zhang, *Rep. Prog. Phys.* **75**, 096501 (2012).
- [50] Y. Ren, Z. Qiao, and Q. Niu, *Rep. Prog. Phys.* **79**, 066501 (2016).
- [51] A. Bansil, H. Lin, and T. Das, *Rev. Mod. Phys.* **88**, 021004 (2016).
- [52] D. J. Rizzo, G. Veber, T. Cao, C. Bronner, T. Chen, F. Zhao, H. Rodriguez, S. G. Louie, M. F. Crommie, and F. R. Fischer, *Nature (London)* **560**, 204 (2018).
- [53] O. Gröning, S. Wang, X. Yao, C. A. Pignedoli, G. B. Barin, C. Daniels, A. Cupo, V. Meunier, X. Feng, A. Narita, K. Muellen, P. Ruffieux, and R. Fasel, *Nature (London)* **560**, 209 (2018).
- [54] W. P. Su, J. R. Schrieffer, and A. J. Heeger, *Phys. Rev. Lett.* **42**, 1698 (1979).
- [55] J. K. Asbóth, L. Oroszlány, and A. Pályi, *A Short Course on Topological Insulators (Band Structure and Edge States in One and Two Dimensions)* (Springer, Berlin, 2015).
- [56] D. J. Rizzo, G. Veber, J. Jiang, R. McCurdy, T. Cao, C. Bronner, T. Chen, S. G. Louie, F. R. Fischer, and M. F. Crommie, *Science* **369**, 1597 (2020).
- [57] Y.-W. Son, M. L. Cohen, and S. G. Louie, *Phys. Rev. Lett.* **97**, 216803 (2006).
- [58] E. J. Meier, F. A. An, and B. Gadway, *Nat. Commun.* **7**, 13986 (2016).
- [59] R. Drost, T. Ojanen, A. Harju, and P. Liljeroth, *Nat. Phys.* **13**, 668 (2017).
- [60] L. Yan and P. Liljeroth, *Adv. Phys.: X* **4**, 1651672 (2019).
- [61] A. Saxena, Y. Chen, Z. Fang, and A. Majumdar, [arXiv:2106.14325](https://arxiv.org/abs/2106.14325).
- [62] A. Coutant, A. Sivadon, L. Zheng, V. Achilleos, O. Richoux, G. Theocharis, and V. Pagneux, *Phys. Rev. B* **103**, 224309 (2021).
- [63] B. G.-g. Chen, N. Upadhyaya, and V. Vitelli, *Proc. Natl. Acad. Sci. USA* **111**, 13004 (2014).
- [64] S. D. Huber, *Nat. Phys.* **12**, 621 (2016).
- [65] Q. Sun, Y. Yan, X. Yao, K. Müllen, A. Narita, R. Fasel, and P. Ruffieux, *J. Phys. Chem. Lett.* **12**, 8679 (2021).
- [66] J. Li, S. Sanz, N. Merino-Diez, M. Vilas-Varela, A. Garcia-Lekue, M. Corso, D. G. de Oteyza, T. Frederiksen, D. Pena, and J. Ignacio Pascual, *Nat. Commun.* **12**, 5538 (2021).
- [67] H.-H. Lin, T. Hikihara, H.-T. Jeng, B.-L. Huang, C.-Y. Mou, and X. Hu, *Phys. Rev. B* **79**, 035405 (2009).
- [68] A. H. Castro Neto, F. Guinea, N. M. R. Peres, K. S. Novoselov, and A. K. Geim, *Rev. Mod. Phys.* **81**, 109 (2009).
- [69] Note that, to improve readability, we show just the negative energies. In addition, to facilitate comparison with Fig. 2, in (a) we label bands 1 to 4 accordingly, although they have obviously changed their positions (except for band 3) in relation to Fig. 2.
- [70] R. S. K. Houtsma, J. de la Rie, and M. Stohr, *Chem. Soc. Rev.* **50**, 6541 (2021).
- [71] P. E. Blöchl, *Phys. Rev. B* **50**, 17953 (1994).
- [72] G. Kresse and J. Furthmüller, *Comput. Mater. Sci.* **6**, 15 (1996).
- [73] G. Kresse and J. Furthmüller, *Phys. Rev. B* **54**, 11169 (1996).
- [74] J. Heyd, G. E. Scuseria, and M. Ernzerhof, *J. Chem. Phys.* **118**, 8207 (2003).
- [75] A. V. Krugau, O. A. Vydrov, A. F. Izmaylov, and G. E. Scuseria, *J. Chem. Phys.* **125**, 224106 (2006).
- [76] J. P. Perdew, K. Burke, and M. Ernzerhof, *Phys. Rev. Lett.* **77**, 3865 (1996).